Nano Energy 49 (2018) 625–633

Contents lists available at ScienceDirect

Nano Energy

journal homepage: www.elsevier.com/locate/nanoen

Full paper

Ultrahigh charge density realized by charge pumping at ambient conditions for triboelectric nanogenerators

Liang Xu[a,b,1], Tian Zhao Bu[a,b,1], Xiao Dan Yang[a,b], Chi Zhang[a,b,*], Zhong Lin Wang[a,b,c,*]

[a] CAS Center for Excellence in Nanoscience, Beijing Key Laboratory of Micro-nano Energy and Sensor, Beijing Institute of Nanoenergy and Nanosystems, Chinese Academy of Sciences, Beijing 100083, PR China

[b] School of Nanoscience and Technology, University of Chinese Academy of Sciences, Beijing 100049, PR China

[c] School of Material Science and Engineering, Georgia Institute of Technology, Atlanta, GA 30332, USA

ARTICLE INFO

Keywords:
Floating layer structure
Charge pump
Triboelectric nanogenerator
Charge density
Ambient condition

ABSTRACT

As a promising technology to harvest mechanical energy from environment, triboelectric nanogenerators (TENGs) impose great importance to further enhance the power density, which is closely related to the charge density on the dielectric surface. A few approaches have been proposed to meet the challenge to improve the charge density, while certain preconditions restrict their applications. Here, a facile and universal method using floating layer structure and charge pump is proposed, based on which an integrated self-charge-pumping TENG device is fabricated. The device adopts a floating layer to accumulate and bind charges for electrostatic induction, while a charge pump is devised to pump charges into the floating layer simultaneously. With elaborately designed structures, this device can achieve ultrahigh effective surface charge density of 1020 $\mu C\,m^{-2}$ in ambient conditions, which is 4 times of that of the density corresponding to air breakdown, presenting a simple and robust strategy to greatly enhance the output of TENGs which should be crucial for developing high performance energy harvesting devices and self-powered systems.

1. Introduction

With the increasing demands of distributed power supply for applications like wearable electronics, implantable devices and internet of things [1–6], technologies that can harvest energy locally from environment are been investigated intensively in recent years [7–13]. As a promising energy harvesting technology, triboelectric nanogenerators (TENGs) show merits of low cost, easy fabrication, abundant choice of materials and structures [4,7,14,15], compared to other energy harvesting technologies [8–10,12,13]. The working principle of the TENG is based on the conjugation of triboelectrification and electrostatic induction [14,16]. Its theoretical fundamental can be derived from the Maxwell's displacement current [4]. Previous works have shown the ability of the TENG to harvest mechanical energy from different sources, especially in low frequencies, like human motion, wind, water wave, and infrastructure vibration [2,17–22], demonstrating versatile application potentials for distributive self-powered systems [4].

The practical application of TENGs imposes a challenging requirement to improve the power density of the device, which is closely related to the charge density in that it has a quadratic dependence on the charge density [23,24]. The enhancement of charge density is restricted mainly by two issues for normal TENG devices under certain intensity of contact or rubbing. The first one is the triboelectrification ability of tribomaterial pairs with certain surface topography [25], and another is the discharge induced by air breakdown [26]. In previous studies, great efforts have been conducted to improve the charge density, based on material selection, surface modification, structure optimization or environment control [2,20,25,27–29]. The corona charging is a relative facile method that is widely adopted, which can inject charges into dielectric films to elevate the charge density from under 100 $\mu C\,m^{-2}$ to about 240 $\mu C\,m^{-2}$ [29]. However, the acquired charges are not stable and the dielectric materials are restricted to electrets. High vacuum environment can suppress air breakdown, which can greatly enhance the charge density to 660 $\mu C\,m^{-2}$ for Cu versus polytetrafluoroethylene (PTFE), and 1003 $\mu C\,m^{-2}$ with an extra ferroelectric barium titanate (BT) layer [28]. Still, this method is restricted by high requirements of device packaging.

To develop a facile and universal method to enhance the charge density of TENG devices, an integrated self-charge-pumping TENG (SCP-TENG) device with features of floating layer structure and charge

* Corresponding authors at: CAS Center for Excellence in Nanoscience, Beijing Key Laboratory of Micro-nano Energy and Sensor, Beijing Institute of Nanoenergy and Nanosystems, Chinese Academy of Sciences, Beijing 100083, PR China.

E-mail addresses: czhang@binn.cas.cn (C. Zhang), zlwang@binn.cas.cn (Z.L. Wang).

[1] These authors contribute equally to this work.

https://doi.org/10.1016/j.nanoen.2018.05.011
Received 12 April 2018; Received in revised form 4 May 2018; Accepted 4 May 2018
Available online 08 May 2018
2211-2855/

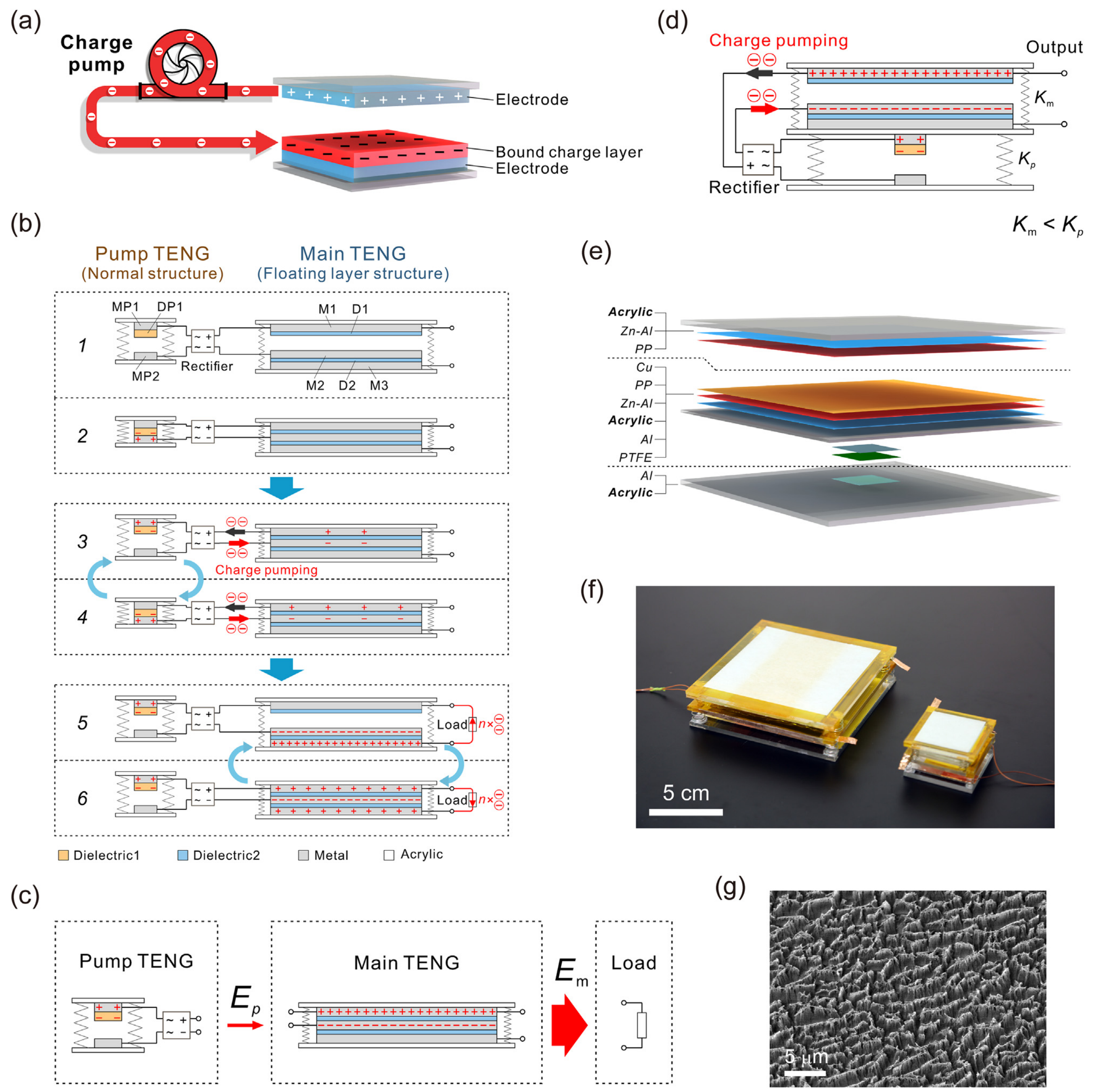

Fig. 1. Device structure and working principle. (a) Schematic diagram of the charge pumping principle. (b) Working process of the floating layer structure with a pump TENG. (c) Schematic of electrical energy transfer among devices and loads. (d) Schematic structure of the integrated device as a self-charge-pumping TENG. (e) Explosive view of the structure and materials of the as-fabricated SCP-TENG. (f) A photograph of as-fabricated SCP-TENGs. (g) A scanning electron microscopy (SEM) image of fabricated nanostructures on the dielectric surface of the pump TENG.

pumping is proposed in this work. Derived from normal TENGs, the proposed device uses a floating layer to store and bind charges for electrostatic induction, while a charge pump is designed to continuously pump charges into the floating layer at the same time. With rationally designed structure, this device can achieve ultrahigh effective surface charge density up to 1020 $\mu C\,m^{-2}$ in ambient conditions, which still has potentials to be further elevated in the near future, presenting a promising strategy to greatly enhance the power output of TENGs for practical applications.

2. Results and discussion

2.1. Structure and working principle

The basic concept of the device is shown in Fig. 1a. A bound charge layer (BCL) and two electrodes are adopted to compose the main part of the device. A conceptual charge pump is set to continuously pump electrons from the upper electrode to the BCL, where the charges are bound without flowing away. The main part of the device is in principle similar to the structure of normal contact-separation-mode TENG except that the bound charges in normal TENG is static charges realized by triboelectrification [7].

To realize the charge-pumping mechanism, we designed a specific device structure as shown in Fig. 1b. The device is composed by two major parts, noted as pump TENG and main TENG, which can conduct contact-separation motion in operation. The pump TENG is essentially a normal TENG, with two metal layers MP1, MP2 and one dielectric layer DP1 that can be effectively triboelectrified [14]. Its alternating charge output is rectified by the rectifier to realize a unidirectional flow of charges, just like a pump to pump charges as proposed above. The main TENG has a different structure, as is mainly consisted of three metal layers M1, M2, M3 and two dielectric layers D1, D2. The M1 and M2 layers are connected to the pump TENG via the rectifier, while the M1 and M3 layers can be connected to external load to output electrical energy. As insulation layers, the D2 layer separates the M2 and the M3 layers, and the D1 layer separates the M1 and the M2 layers while the main TENG is in contact state. Thus the M2 layer does not exchange charges directly with the M1 and the M3 layers which are connected to external loads. In this sense, the M2 layer is a “floating” layer, and it can only accept unidirectional flow of electrons from the rectifier. In case of no dissipation, electrons will accumulate and be bound in the layer to achieve high charge density with continuously charge injection. Therefore, the proposed BCL can be realized. Springs are adopted both in the main TENG and the pump TENG to help to realize the contact-separation motion. Here, although the structure of the main TENG is not a normal one, it is still called “TENG” due to similar working mechanism based on electrostatic induction as will be discussed later [16].

Detailed working process of the whole device with 6 steps is shown in Fig. 1b. Step 1 is the initial state of the device where there is no charge separation in the system and the main TENG and the pump TENG are all in separation state. In step 2, the two parts get into contact state, and due to contact electrification effect, the DP1 layer and the MP2 layer in the pump TENG possess charges of different signs. The contact electrification effect in the main TENG is neglected considering that it is very weak and has litter influence to the performance of the device. In steps 3 and 4, the pump TENG works like a normal TENG. With the rectifier, the alternating charge output of the pump TENG is rectified into a direct one, thus pumps electrons from the M1 layer to the M2 layer. The process is similar to charging a capacitor and the two metal layers can be regarded as the two electrodes of the capacitor. The main TENG is kept in contact state to maximize the capacitance to accommodate more charges when the output voltage of the pump TENG is determined. Such process can last until breakdown of the dielectric layers. With several cycles of steps 3 and 4, considerable charges are accumulated in the floating M2 layer of the main TENG. Then the device can go to steps 5 and 6, when the main TENG conducts contact-separation motion. The charges in the floating layer are bound like static charges in normal TENGs, which can induce charge transferring between the M1 and the M3 layers based on electrostatic induction [16]. In normal TENG, charge density is restricted by the ability of adopted tribo-pairs to lose and gain charges and the rubbing or contact force while not considering breakdown of the air [25]. For the floating layer structure, charge density is only decided by the electrical strength of the dielectric layer and the output voltage of the pump TENG, thus ultrahigh charge density can be expected.

Fig. 1c shows the energy perspective of the device. The pump TENG as a self-powered charge source provides a small amount of energy E_p to pump charges, and the effect of such energy is added up by charge accumulation, establishing high charge density and strong electrical field in the main TENG. This greatly enhance the power and energy harvesting ability of the main TENG [23,24]. Thus high output electrical energy E_m can be provided to drive external loads. As the high charge density does not rely on intensive rubbing or contact which can be accompanied by heat generation and abrasion with lots of extra energy consumption, the total efficiency of the device should be high.

For practical applications, the above structures and processes are integrated as a self-charge-pumping TENG, as shown in Fig. 1d. The main TENG and the pump TENG are stacked up, with the stiffness of the spring in the main TENG K_m smaller than that in the pump TENG K_p. In this context, the SCP-TENG has the working process as shown in Fig. S1. Due to that $K_m < K_p$, the main TENG will get into contact state before the pump TENG upon pressing and get out of the contact state after the pump TENG in the release step. This is to say, the main TENG keeps in contact state for most of the contact-separation process of the pump TENG, as can improve the charge pumping effect as discussed above. This SCP-TENG can operate like normal TENG with simple press-release actions, while stimulating bound charges to ultrahigh density.

As-fabricated SCP-TENG devices are shown in Fig. 1f. Fig. 1e provides the structure and materials for the fabricated devices. The dielectric material is polypropylene (PP) for the main TENG and PTFE for the pump TENG. As is well known, PTFE has strong ability to be triboelectrified, which is further enhanced by fabrication of nanostructures on its surface as shown in Fig. 1g [30]. Detailed fabrication process of the device is illustrated in the experimental section.

2.2. Theoretical model

To better understand the working mechanism of the floating layer

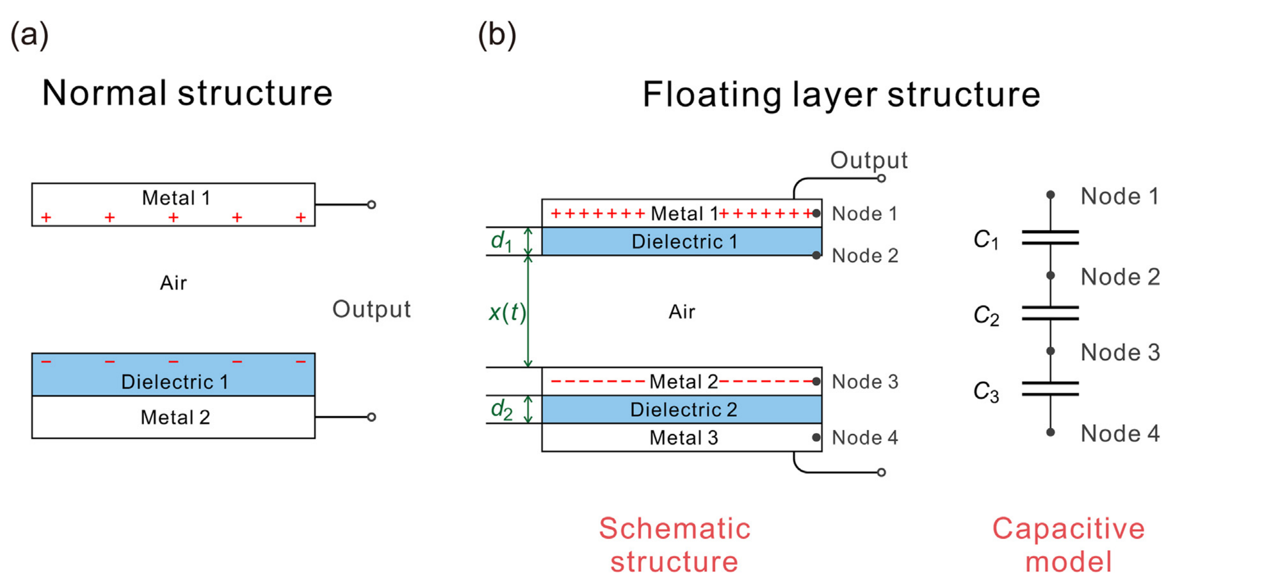

Fig. 2. Theoretical model of the floating layer structure. (a) Schematic structure of the corresponding normal TENG. (b) Schematic structure and capacitive model of the floating layer structure device.

structure and the SCP-TENG device, a theoretical model is established. The floating layer structure can be regarded as a derivation from normal conductor-to-dielectric contact-separation-mode TENG, as shown in Fig. 2. For the normal TENG in Fig. 2a, it has two metal electrodes and a dielectric layer, where the two electrodes are connected to output, and the dielectric layer binds static charges. For the floating layer structure in Fig. 2b, such dielectric layer is substituted by a metal layer isolated by two dielectric layers from the two electrodes. As a floating layer, it can also bind charges in the layer, while the charge density can be greatly enhanced. The floating layer structure can be theoretically analyzed according to a proposed electrodynamics method [16,31]. First, it can be assumed that the charge density in Metal 2 is $-\sigma$, the area of each layer is S and the amount of charges transferred into Metal 3 is Q. Metal 1 plays two roles: both as the sources for charge pumping and for charges transferring to Metal 3. From charge conservation, the charge amount in Metal 1 is $S\sigma$-Q. Then based on the Gauss theorem, the V–Q–x relationship for this model is given by

$$V = -\frac{Q}{S\varepsilon_0}\left(\frac{d_1}{\varepsilon_{r1}} + \frac{d_2}{\varepsilon_{r2}} + x(t)\right) + \frac{\sigma}{\varepsilon_0}\left(\frac{d_1}{\varepsilon_{r1}} + x(t)\right) \tag{1}$$

where V is the voltage between Metal 1 and Metal 3, x is the separation distance between Dielectric 1 and Metal 2, ε_{r1}, ε_{r2} are relative permittivities of the two dielectric layers, ε_0 is the permittivity of air, d_1, d_2 are thicknesses of the two dielectric layers. Eq. (1) can be further transformed into a capacitance form based on the capacitive model shown in Fig. 2b. In short-circuit condition where $V = 0$, the amount of charges in Metal 3 is given by

$$Q = \frac{S\sigma\left(\frac{1}{C_1} + \frac{1}{C_2}\right)}{\frac{1}{C_1} + \frac{1}{C_2} + \frac{1}{C_3}} \tag{2}$$

When x is changing from 0, the short-circuit transferred charges from Metal 1 to Metal 3 (Q_{CT}) can be given by

$$Q_{CT} = \frac{S\sigma\left(\frac{1}{C_1(x)} + \frac{1}{C_2(x)}\right)}{\frac{1}{C_1(x)} + \frac{1}{C_2(x)} + \frac{1}{C_3(x)}} - \frac{S\sigma\left(\frac{1}{C_1(x=0)} + \frac{1}{C_2(x=0)}\right)}{\frac{1}{C_1(x=0)} + \frac{1}{C_2(x=0)} + \frac{1}{C_3(x=0)}} \tag{3}$$

The charge transfer efficiency η_{CT}, which is defined as the ratio of the final transferred charges at x_{max} and the total injected charges into the floating layer, can be calculated as

$$\eta_{CT} = \frac{Q_{CT,final}}{S\sigma} = \frac{\left(\frac{1}{C_1(x=x_{max})} + \frac{1}{C_2(x=x_{max})}\right)}{\frac{1}{C_1(x=x_{max})} + \frac{1}{C_2(x=x_{max})} + \frac{1}{C_3(x=x_{max})}} - \frac{\left(\frac{1}{C_1(x=0)} + \frac{1}{C_2(x=0)}\right)}{\frac{1}{C_1(x=0)} + \frac{1}{C_2(x=0)} + \frac{1}{C_3(x=0)}} \tag{4}$$

The above theoretical equations of the floating layer structure has similar forms as normal TENG [16], showing that they should be based on analogical principles. Details of the deduction procedure can be referred to the Supplementary information. It is easy to speculate that for dielectric-to-dielectric contact-separation-mode TENG, there is also a corresponding structure with double floating layers, which is discussed in the Supplementary information.

2.3. Performance characterization

To test the performance of individual floating layer structure, a

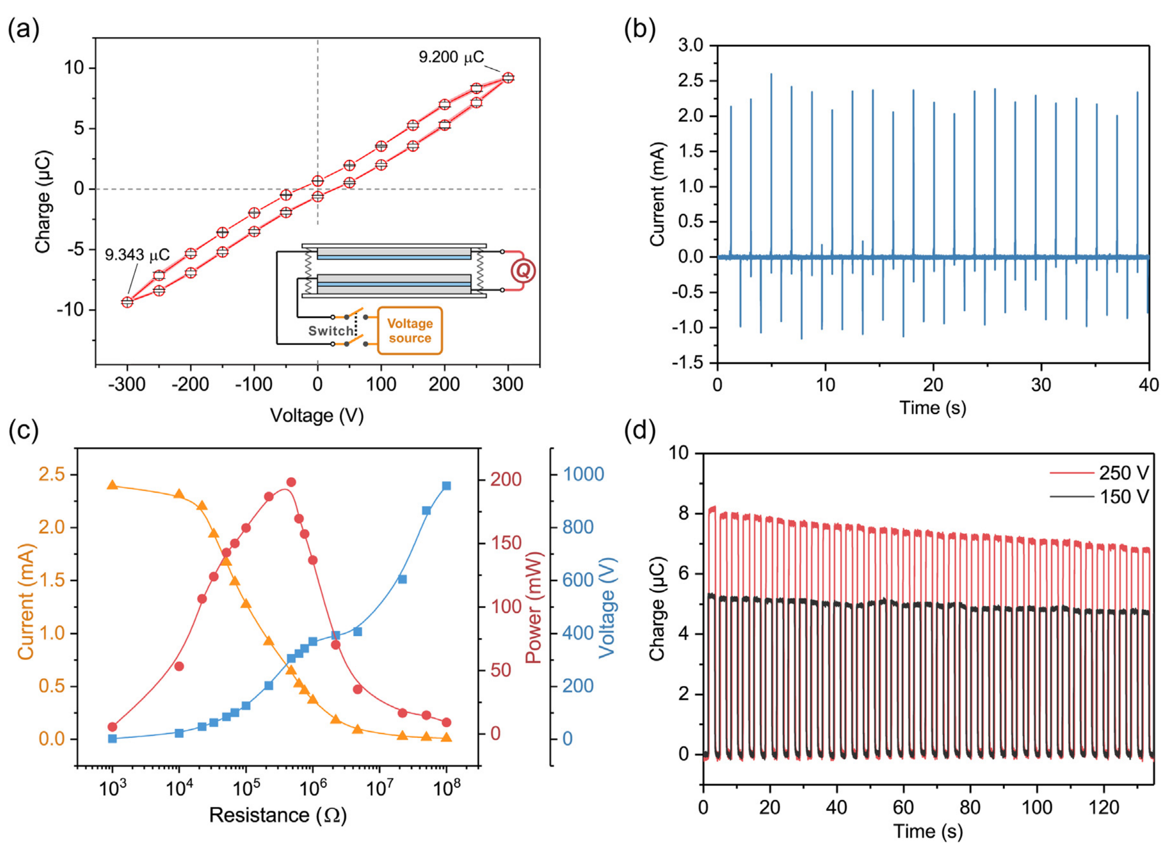

Fig. 3. Electrical output characteristics of the floating layer structure initialized by a voltage source. (a) Short-circuit transferred charges under different initializing voltages. Inlet: electrical circuit for the experiments. (b) Short-circuit current with an initializing voltage of 250 V. (c) Dependence of the output current, voltage and peak power on different resistive loads. (d) Decay of the charge output for different initializing voltages.

commercial voltage source was adopted to inject charges into the floating layer, which can act like a charge pump with controllable voltage. Such voltage should be proportional to the injected charges considering the capacitance do not vary in the contact state, and opposite voltages would cause injection of opposite signs of charges. The measurement setup and process are shown in the inlet of Figs. 3a and S3. First, the voltage source was connected to the M1 and M2 layers to apply certain initializing voltage, which was then cut off before conducting contact-separation motions. The output from the M1 and M3 layers was measured. Fig. 3a shows the short-circuit transferred charges for the floating layer structure with an active area of 10 × 10 cm^2, under gradually changed voltage cycling from − 300 to 300 V then back to − 300 V. The charge output increase almost linearly with the voltage and can reach 9.343 μC at − 300 V, corresponding to an ultrahigh charge density of 934.3 μC m^{-2}. The area enclosed by the curve shows a week polarization effect of the dielectric layer, which can induce non-zero output with applied voltage of 0 V. Moreover, the amount of transferred charges show little difference for opposite signs of injected charges in the floating layer under opposite voltages. The experiments also imply that the output charges of the device can be precisely controlled by the applied voltage. The short-circuit current by an initializing voltage of 250 V reaches 2.4 mA under a contact-separation frequency of 0.5 Hz, as shown in Fig. 3b. The dependence of the output on a resistive load is presented in Fig. 3c. A maximum peak power of 198 mW can be achieved under a resistance of 474 kΩ, corresponding to a power density of 19.8 W m^{-2}. The charges in the floating layer could gradually dissipate to surrounding environment due to the high potential in the working process [32]. Fig. 3d shows decay of charge output related with such dissipation. For both initializing voltage of 250 V and 150 V, the decay is slow, from 8.16 μC to 6.90 μC (about 15%) for 250 V and from 5.27 μC to 4.75 μC (about 9.9%) for 150 V in 120 s. Thus the bound charge will last for a relative long time in the floating layer, benefiting charge accumulation with charge pumping.

The performance of the integrated SCP-TENG was then characterized without any extra voltage source. Pump TENGs with different active areas were used in the experiments. Fig. 4a shows the transferred charges for pump TENGs with three different active areas, while Fig. 4b shows the increasing voltage of the floating layer accompanying the charge injection by different pump TENGs. For the middle-sized pump TENG with an active area of 4 × 4 cm^2, the transferred charges is 131 nC, and it can charge the floating layer to 200 V in 55 s with a contact-separation frequency of 1.3 Hz. The open-circuit voltage of the pump TENG was also measured as shown in Fig. S4 in the Supplementary information. Fig. 4c demonstrates the transferred charges of the SCP-TENG from the very beginning. For each size of pump TENG, the output has the same variation trend. The upper and lower limits of the charge curve both increase with time, and the difference between them also rise rapidly, which corresponds to the transferred charges in each contact-separation cycle. With larger pump TENG size, the

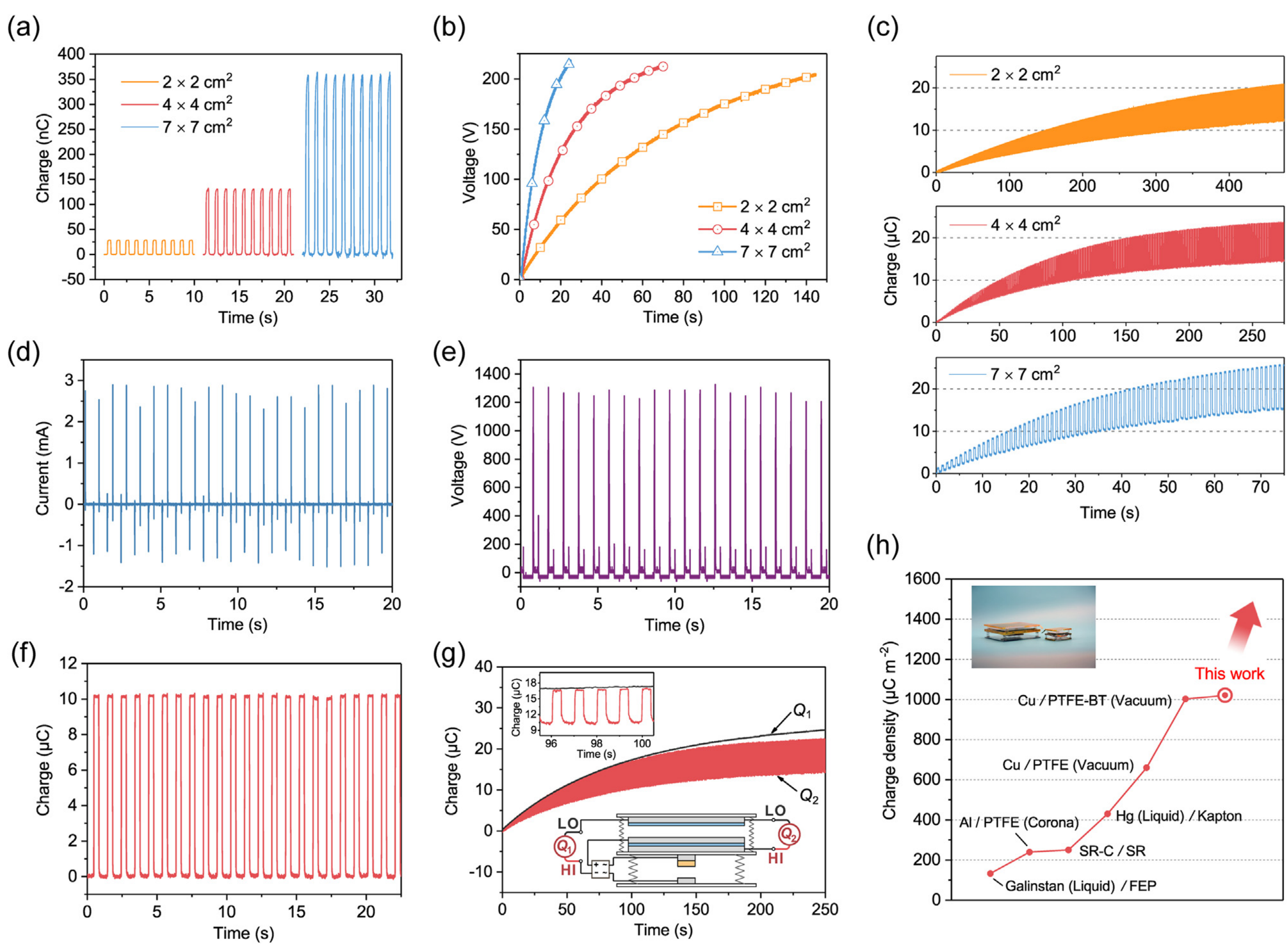

Fig. 4. Electrical output characteristics of the SCP-TENG. (a) Short-circuit transferred charges for pump TENGs with different sizes. (b) Voltage of the floating layer in contact state under charge pumping. (c) Enhancing process of the short-circuit transferred charges of the SCP-TENG by pump TENGs with different sizes. (d-f) Typical short-circuit current, rectified voltage and shifted transferred charges of the SCP-TENG. (g) The pumped charges and the output transferred charges for the same SCP-TENG with a pump TENG of 4 × 4 cm^2. Measured data of Q_1 are flipped from negative to positive for comparison with Q_2. Inlet: the enlarged view and the measurement circuit, where HI and LO mark the "input high" and "input low" terminals of the electrometer respectively. (h) Ultrahigh charge density realized in ambient conditions by this work, which also offers possibility for even higher charge density.

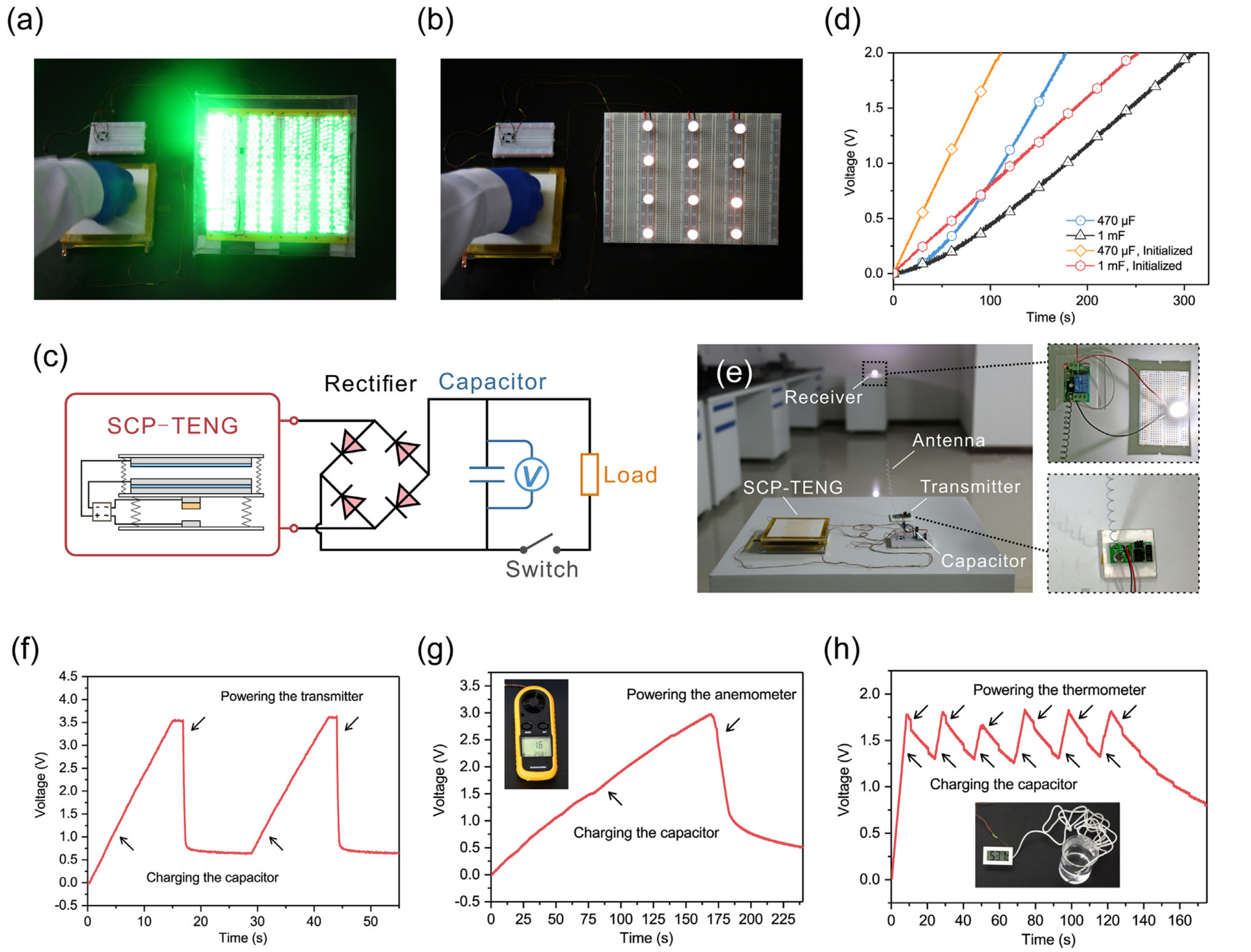

Fig. 5. Demonstrations of the SCP-TENG to drive electrical loads. (a) Directly powering 600 LEDs. (b) Directly driving large LED bulbs. (c) Schematic diagram of the electrical circuit to charge a capacitor for electronic devices. (d) Charging performance of the SCP-TENG for different capacitances. (e, f) Photographs and charge-discharge curve for the SCP-TENG to drive a wireless transmitter. (g, h) Charge-discharge curves for the SCP-TENG to power an anemometer (g) and a thermometer (h). Inlets show the powered anemometer and thermometer respectively.

increase process is more rapid. With pump TENG of $4 \times 4\,cm^2$, the transferred charges increase from 0 to 8.65 μC in 200 s under a contact-separation frequency of 1 Hz. This implies that the charges are accumulating continuously in the floating layer. Even with very small active area of $2 \times 2\,cm^2$, the pump TENG can still work effectively to pump charges into the floating layer. It can also be observed that the rate of charge rising decreases slowly, consistent with the voltage curve in Fig. 4b. This can be attributed to lower efficiency to inject charges with increasing voltage of the floating layer, just like the behavior of a capacitor. Such experiment process for the charge output enhancement is also shown in Video S1 in the Supplementary information. Typical short-circuit current, voltage and transferred charges for the SCP-TENG are shown in Fig. 4d-f. The short-circuit current of the SCP device with a pump TENG of $4 \times 4\,cm^2$ can reach 2.88 mA under a contact-separation frequency of 1 Hz, and the peak voltage is 1290 V. The transferred charges of the SCP device with a pump TENG of $7 \times 7\,cm^2$ can achieve 10.2 μC, corresponding to an ultrahigh charge density of $1020\,\mu C\,m^{-2}$ while considering the area of the floating layer. Fig. 4h shows typical values of charge density achieved for TENGs [2,24,28,29,33]. Liquid Galinstan versus fluorinated ethylene propylene (FEP) has a density of about $133\,\mu C\,m^{-2}$ [24]. Corona charging is a common and effective method to enhance charge density, showing a value of $240\,\mu C\,m^{-2}$ [29]. For silicon rubber mixed with carbon versus silicon rubber (SR-C/SR), the value is $250\,\mu C\,m^{-2}$ [2]. With liquid Hg versus Kapton, the value can be improved to $430\,\mu C\,m^{-2}$ [33]. High vacuum environment can suppress electrostatic breakdown of the air, thus can greatly raise the charge density to a high level of $660\,\mu C\,m^{-2}$ for Cu versus PTFE, and $1003\,\mu C\,m^{-2}$ with an extra ferroelectric barium titanate layer [28]. This work further improves the value to $1020\,\mu C\,m^{-2}$ for devices with large contact sizes, as is calculated from the output charges. Such charge density is 4 times of the density corresponding to air breakdown [28], which can be attributed to the insulation and protection of the dielectric layers. If referring to the stored charges in the floating layer, the charge density should be even higher. The work also provides a promising strategy for even higher performance in the future. More importantly, such high charge density is achieved in facile conditions which can be universally applied in various applications, while in comparison, other methods usually have certain preconditions like high vacuum, liquid metal or corona charging that are sometimes not easy to apply.

Supplementary material related to this article can be found online at http://dx.doi.org/10.1016/j.nanoen.2018.05.011.

To further verify the working mechanism of the SCP-TENG, the pumped charges Q_1 and the output transferred charges Q_2 were measured according to the setup shown in the inlet of Fig. 4g. It can be observed that Q_1 increases monotonously with time while Q_2 has an oscillating feature. At beginning, the upper limit of Q_2 coincides well with Q_1, and the lower limit of Q_2 does not return to zero. This is consistent with the proposed theoretical model. In the separation process with large enough distance, all positive charges are transferred to the M3 layer of the main TENG, which is equal to the negative charges injected into the M2 layer. Whereas in the contact state, due to the existence of the D1 layer, the M1 and the M2 layers cannot get close enough to maximize corresponding capacitance, thus the charge transfer efficiency cannot achieve 100% according to Eq. (4). In the experiments, C_1 and C_3 is measured as 29 nF and 43 nF respectively. C_2 is infinitely large at $x = 0$ and nearly zero for $x = x_{\max}$ where $x_{\max}$ is sufficiently large. Based on Eq. (4), the charge transfer efficiency η_{CT} can be calculated as 40%. For comparison, the efficiency directly derived from charge measurement shown in Fig. 4g is 38%, which coincides well with the above theoretical prediction. Another noticeable phenomenon is that Q_1 gradually deviates from the upper limit of Q_2 with increasing amount of injected charges. This can be attributed to the charge dissipation with time under high voltage as discussed previously. The durability of such device is also tested, as shown in Fig. S5. Upon continuous test of one hour, the device can maintain high output, showing good stability.

2.4. Demonstrations of application

Due to that the output power density has a quadratic relationship with the charge density, the power of the SCP-TENG can be greatly enhanced with such ultrahigh charge density in ambient conditions, enabling highly effective energy harvesting for various applications. First, as intuitive demonstrations, the device were used to power large amounts of LED devices, as shown in Fig. 5a, b and Videos S2-S4 in the Supplementary information. The SCP-TENG can effectively light 600 small LEDs or 12 large LED bulbs to high brightness. The electricity output by the SCP-TENG can also be stored in capacitors or batteries based on a circuit shown in Fig. 5c. The current from the device is first rectified, then supplied for a capacitor, which can store the energy and power external loads afterwards. The charging performance of the SCP-TENG device with a pump TENG of $4 \times 4\ \mathrm{cm}^2$ for different capacitances is shown in Fig. 5d. For the device without any charges in the floating layer, it needs a few time to be initialized to reach considerable output, thus the charging rate has a variation from low to high. For devices that are already initialized at the beginning, the charging can maintain at high rate. A capacitor of 470 μF can be charged to 2 V in 110 s with a contact-separation frequency of 1 Hz. Fig. 5e-h further demonstrate applications of the SCP-TENG as an effective power source to drive various electronic devices. In Fig. 5e, a pair of wireless transmitter and receiver was placed with a distance of 5 m. After the capacitor of 220 μF was charged from 0 V to about 3.5 V in 15 s, the switch was closed and the transmitter was powered up to send a signal to the receiver, which then turned on a LED bulb based on the signal. The voltage variation of the capacitor for two consequent transmitting process is shown in Fig. 5f. Similarly, demonstrations for the SCP-TENG to power an anemometer and a thermometer are shown in Fig. 5g and h, where the adopted capacitors are 1 mF and 220 μF respectively. The experiment processes of the wireless transmission and the thermometer are also shown in Video S5 and S6 in the Supplementary information.

Supplementary material related to this article can be found online at http://dx.doi.org/10.1016/j.nanoen.2018.05.011.

As demonstrated above, the SCP-TENG represents an effective strategy to reach ultrahigh charge density and power for the TENG device. Compared to normal structures, the charge generation does not rely on intensive friction between two surfaces, which could induce abrasion and heat generation, affecting the durability and efficiency of the device. The charge density in the SCP-TENG is decided by the accumulation of the injected charges, thus very little charge injection can produce large output with time, showing superior advantages in comparison to normal TENG. The facile availability of this method in various application conditions also prevails other reported charge density enhancement methods [28,29,33]. Although the device here is based on a contact-separation mode, it is also possible to design similar structures to enhance the output of TENGs with other modes [14,16].

As is well known, the application of electromagnets, which use electricity to excite magnetic field, is crucial for electro-magnetic generators. The SCP-TENG using injected bound charges instead of friction-agitated static charges to excite electric field, should have similar importance for further development of the TENG and energy harvesting research.

3. Conclusions

In summary, an integrated self-charge-pumping TENG with floating layer structure and a charge pump is proposed. By pumping charges into the floating layer with a TENG based charge pump, the SCP-TENG can operate like normal TENGs, while accumulating bound charges with high efficiency to ultrahigh effective surface density of $1020\ \mu\mathrm{C\,m}^{-2}$ in ambient conditions, as is the highest compared to reported results. More importantly, this method is rather facile and robust compared to other charge density enhancing approaches, providing an important strategy to improve the output of TENG devices, which is crucial for various practical applications ranging from wearable electronics to blue energy.

4. Experimental section

4.1. Fabrication of the nanostructures on PTFE surface

First, a thin layer of copper was deposited onto a 50 μm thick PTFE film. Then inductively coupled plasma (ICP) etching (SENTECH SI-500) was applied to fabricate nanostructures on the surface of PTFE. O_2, Ar and CF_4 gases were injected into the ICP chamber with flow rates of 10.0, 15.0 and 30.0 sccm (standard cubic centimeter per minute), respectively. The plasma was generated by a power source of 400 W. And another power source of 100 W was used to accelerate the plasma. The copper-coated PTFE film was etched for 10 min to get nanostructures.

4.2. Fabrication of the main TENG

To fabricate the main TENG, two pieces of acrylic were cut as substrates by a laser cutter with dimensions of 120 mm × 120 mm × 3 mm. Four blind holes were carved at each corner for spring installation. For the bottom substrate, a layer of 100 mm × 100 mm × 3 mm silicone rubber (Ecoflex 00–20) was casted onto the acrylic by mixing the base and the curing agent in 1:1 weight ratio to form a soft substrate (not shown in Fig. 1e for simplicity), which was cured at room temperature for at least 4 h. A 5 μm thick PP film which is single-side coated with Zn-Al was adhered on the silicone rubber with the Zn-Al side to the silicone rubber, and then a copper layer of 100 nm was deposited on the non-coated side of the PP film. For the top substrate, another Zn-Al coated PP film was assembled on the acrylic substrate with the non-coated side facing the bottom substrate. Finally, four springs were anchored to connect the top and the bottom substrates.

4.3. Fabrication and integration of the pump TENG

A piece of Al foil covered by the prepared nanostructured PTFE film was adhered on the opposite side of the bottom substrate of the main TENG. Then, a bare Al foil was adhered on another as-prepared acrylic substrate. Four springs with higher stiffness were anchored on substrates to connect the pump TENG.

4.4. Measurement of the device

The output voltage of the SCP-TENG was measured by a digital oscilloscope (Tektronix MDO 3024 & Tektronix P6015A). The voltage of the capacitor, the transferred charges and the current were measured by an electrometer (Keithley 6514). The open-circuit voltage of pump TENGs was measured by an electrostatic voltmeter (Trek 344). A source meter (Keithley 2410) was adopted as the voltage source for testing the floating layer structure without the pump TENG.

Acknowledgements

We would like to thank Jian Jun Luo for taking SEM images of the nanostructures. Research was supported by the National Key R & D Project from Minister of Science and Technology, China (2016YFA0202704), National Natural Science Foundation of China (Grant No. 51605033, 51432005, 5151101243, and 51561145021), the "Thousands Talents" Program for Pioneer Researcher and His Innovation Team, China, China Postdoctoral Science Foundation (Grant No. 2015M581041), Beijing Talents Foundation (2017000021223TD04), Beijing Nova Program (Grant No. Z171100001117054) and Beijing Municipal Science & Technology Commission (Grant No. Z171100000317001).

Appendix A. Supporting information

Supplementary data associated with this article can be found in the online version at http://dx.doi.org/10.1016/j.nanoen.2018.05.011.

References

[1] S.H. Wang, J. Xu, W.C. Wang, G.J.N. Wang, R. Rastak, F. Molina-Lopez, J.W. Chung, S.M. Niu, V.R. Feig, J. Lopez, T. Lei, S.K. Kwon, Y. Kim, A.M. Foudeh, A. Ehrlich, A. Gasperini, Y. Yun, B. Murmann, J.B.H. Tok, Z.A. Bao, Nature 555 (2018) 83–88.
[2] J. Wang, S.M. Li, F. Yi, Y.L. Zi, J. Lin, X.F. Wang, Y.L. Xu, Z.L. Wang, Nat. Commun. 7 (2016) 12744.
[3] Q. Zheng, Y. Zou, Y.L. Zhang, Z. Liu, B.J. Shi, X.X. Wang, Y.M. Jin, H. Ouyang, Z. Li, Z.L. Wang, Sci. Adv. 2 (2016) e1501478.
[4] Z.L. Wang, Mater. Today 20 (2017) 74–82.
[5] Q.L. Hua, J.L. Sun, H.T. Liu, R.R. Bao, R.M. Yu, J.Y. Zhai, C.F. Pan, Z.L. Wang, Nat. Commun. 9 (2018) 244.
[6] S.M. Niu, X.F. Wang, F. Yi, Y.S. Zhou, Z.L. Wang, Nat. Commun. 6 (2015) 8975.
[7] F.R. Fan, Z.Q. Tian, Z.L. Wang, Nano Energy 1 (2012) 328–334.
[8] Z.L. Wang, J.H. Song, Science 312 (2006) 242–246.
[9] G.B. Xue, Y. Xu, T.P. Ding, J. Li, J. Yin, W.W. Fei, Y.Z. Cao, J. Yu, L.Y. Yuan, L. Gong, J. Chen, S.Z. Deng, J. Zhou, W.L. Guo, Nat. Nanotechnol. 12 (2017) 317–321.
[10] S.H. Kim, C.S. Haines, N. Li, K.J. Kim, T.J. Mun, C. Choi, J.T. Di, Y.J. Oh, J.P. Oviedo, J. Bykova, S.L. Fang, N. Jiang, Z.F. Liu, R. Wang, P. Kumar, R. Qiao, S. Priya, K. Cho, M. Kim, M.S. Lucas, L.F. Drummy, B. Maruyama, D.Y. Lee, X. Lepro, E.L. Gao, D. Albarq, R. Ovalle-Robles, S.J. Kim, R.H. Baughman, Science 357 (2017) 773–778.
[11] J.D. Feng, M. Graf, K. Liu, D. Ovchinnikov, D. Dumcenco, M. Heiranian, V. Nandigana, N.R. Aluru, A. Kis, A. Radenovic, Nature 536 (2016) 197–200.
[12] L.D. Zhao, G.J. Tan, S.Q. Hao, J.Q. He, Y.L. Pei, H. Chi, H. Wang, S.K. Gong, H.B. Xu, V.P. Dravid, C. Uher, G.J. Snyder, C. Wolverton, M.G. Kanatzidis, Science 351 (2016) 141–144.
[13] A. Fakharuddin, R. Jose, T.M. Brown, F. Fabregat-Santiago, J. Bisquert, Energ. Environ. Sci. 7 (2014) 3952–3981.
[14] Z.L. Wang, J. Chen, L. Lin, Energy Environ. Sci. 8 (2015) 2250–2282.
[15] Z.L. Wang, Faraday Discuss. 176 (2014) 447–458.
[16] S.M. Niu, Z.L. Wang, Nano Energy 14 (2015) 161–192.
[17] Y. Zi, H. Guo, Z. Wen, M.H. Yeh, C. Hu, Z.L. Wang, ACS Nano 10 (2016) 4797–4805.
[18] Z.L. Wang, Nature 542 (2017) 159–160.
[19] L. Xu, Y.K. Pang, C. Zhang, T. Jiang, X.Y. Chen, J.J. Luo, W. Tang, X. Cao, Z.L. Wang, Nano Energy 31 (2017) 351–358.
[20] L. Xu, T. Jiang, P. Lin, J.J. Shao, C. He, W. Zhong, X.Y. Chen, Z.L. Wang, ACS Nano 12 (2018) 1849–1858.
[21] J. Bae, J. Lee, S. Kim, J. Ha, B.S. Lee, Y. Park, C. Choong, J.B. Kim, Z.L. Wang, H.Y. Kim, J.J. Park, U.I. Chung, Nat. Commun. 5 (2014) 4929.
[22] H. Yu, X. He, W.B. Ding, Y.S. Hu, D.C. Yang, S. Lu, C.S. Wu, H.Y. Zou, R.Y. Liu, C.H. Lu, Z.L. Wang, Adv. Energy Mater. 7 (2017) 1700565.
[23] S.H. Wang, Y.N. Xie, S.M. Niu, L. Lin, C. Liu, Y.S. Zhou, Z.L. Wang, Adv. Mater. 26 (2014) 6720–6728.
[24] Y.L. Zi, S.M. Niu, J. Wang, Z. Wen, W. Tang, Z.L. Wang, Nat. Commun. 6 (2015) 8376.
[25] C. Zhang, W. Tang, C.B. Han, F.R. Fan, Z.L. Wang, Adv. Mater. 26 (2014) 3580–3591.
[26] Y.L. Zi, C.S. Wu, W.B. Ding, Z.L. Wang, Adv. Funct. Mater. 27 (2017) 1700049.
[27] H.Y. Li, L. Su, S.Y. Kuang, C.F. Pan, G. Zhu, Z.L. Wang, Adv. Funct. Mater. 25 (2015) 5691–5697.
[28] J. Wang, C.S. Wu, Y.J. Dai, Z.H. Zhao, A. Wang, T.J. Zhang, Z.L. Wang, Nat. Commun. 8 (2017) 88.
[29] T. Zhou, L.M. Zhang, F. Xue, W. Tang, C. Zhang, Z.L. Wang, Nano Res. 9 (2016) 1442–1451.
[30] H. Fang, W.Z. Wu, J.H. Song, Z.L. Wang, J. Phys. Chem. C 113 (2009) 16571–16574.
[31] S.M. Niu, S.H. Wang, L. Lin, Y. Liu, Y.S. Zhou, Y.F. Hu, Z.L. Wang, Energy Environ. Sci. 6 (2013) 3576–3583.
[32] X.Y. Chen, D. Taguchi, T. Manaka, M. Iwamoto, Z.L. Wang, Sci. Rep. 5 (2015) 13019.
[33] W. Tang, T. Jiang, F.R. Fan, A.F. Yu, C. Zhang, X. Cao, Z.L. Wang, Adv. Funct. Mater. 25 (2015) 3718–3725.

Dr. Liang Xu received his Ph.D. degree from Tsinghua University (THU) in 2012, with awards of Excellent Doctoral Dissertation of THU and Excellent Graduate of Beijing. Before that he achieved bachelor's degree of mechanical engineering in Huazhong University of Science & Technology (HUST) in 2007. He is now a postdoctoral fellow in Beijing Institute of Nanoenergy and Nanosystems, Chinese Academy of Sciences (CAS), under the supervision of Prof. Zhong Lin Wang. His research interests include nanogenerators and self-powered nanosystems, blue energy, fundamental tribological phenomena, scanning probe microscopy and molecular dynamics simulation.

Tian Zhao Bu received his undergraduate degree in Material Science and Engineering from Zhengzhou University, China in 2015, and now he is a doctoral candidate in Beijing Institute of Nanoenergy and Nanosystems, Chinese Academy of Sciences. His research interests are mainly focused on triboelectric nanogenerator and tribotronics, especially focus on the functional tribotronic devices and their applications in sensor networks and human machine interaction.

Xiao Dan Yang received her Bachelor of Science in Xidian University in 2016. She is currently pursuing a master's degree in Beijing Institute of Nanoenergy and Nanosystems under the supervision of Prof. Zhong Lin Wang. Her research interests include blue energy and self-powered electronics.

Prof. Chi Zhang received his Ph.D. degree from Tsinghua University in 2009. After graduation, he worked in Tsinghua University as a postdoc research fellow and NSK Ltd., Japan as a visiting scholar. He now is the principal investigator of Tribotronics Group in Beijing Institute of Nanoenergy and Nanosystems, Chinese Academy of Sciences (CAS), Fellow of the NANOSMAT Society, Member of Youth Innovation Promotion Association, CAS, and Youth Working Committee Member of Chinese Society of Micro-Nano Technology. Prof. Chi Zhang's research interests are triboelectric nanogenerator, tribotronics, self-powered MEMS/NEMS, and applications in sensor networks, human-computer interaction and new energy technology. He has been awarded by NSK Sino-Japan Friendship Excellent Paper Award of Mechanical Engineering and granted by National Natural Science Foundation of China, Beijing Municipal Science & Technology Commission, Beijing Natural Science Foundation, China Postdoctoral Science Foundation, and CAS. He has published over 70 papers and attained 24 patents. Details can be found at: www.binn.cas.cn/ktz/zcyjz/yjzjzc/

Prof. Zhong Lin Wang received his Ph.D. from Arizona State University in physics. He now is the Hightower Chair in Materials Science and Engineering, Regents' Professor, Engineering Distinguished Professor and Director, Center for Nanostructure Characterization, at Georgia Tech. Prof. Wang has made original and innovative contributions to the synthesis, discovery, characterization and understanding of fundamental physical properties of oxide nanobelts and nanowires, as well as applications of nanowires in energy sciences, electronics, optoelectronics and biological science. His discovery and breakthroughs in developing nanogenerators established the principle and technological roadmap for harvesting mechanical energy from the environment and biological systems for powering a personal electronics. His research on self-powered nanosystems has inspired the worldwide effort in academia and industry for studying energy for micro-nano-systems, which is now a distinct disciplinary in energy research and future sensor networks. He coined and pioneered the field of piezotronics and piezophototronics by introducing piezoelectric potential gated charge transport process in fabricating new electronic and optoelectronic devices. Details can be found at: www.nanoscience.gatech.edu.